Nuclear Engineering and Technology 56 (2024) 2595–2609

Contents lists available at ScienceDirect

Nuclear Engineering and Technology

journal homepage: www.elsevier.com/locate/net

Original Article

Investigations on seismic performance of nuclear power plants equipped with an optimal BIS-TMDI considering FSI effects

Shuaijun Zhang [a], Gangling Hou [a], Chengyu Yang [b], Zhihua Yue [c], Yuzhu Wang [a], Min He [a], Lele Sun [a], Xuesong Cai [a,*]

[a] Yantai Research Institute of Harbin Engineering University, Harbin Engineering University, Yantai 264006, China
[b] State Key Laboratory of Disaster Reduction in Civil Engineering, Tongji University, Shanghai 200092, China
[c] College of Aerospace and Civil Engineering, Harbin Engineering University, Harbin 150000, China

ARTICLE INFO

Keywords:
Hybrid vibration control
Optimal design
Fluid-structure interaction
AP1000

ABSTRACT

This paper introduces a base isolation system-tuned mass damper inerter (BIS-TMDI) hybrid system to the AP1000 nuclear power plant (NPP), which reduces seismic damage potential of the NPP structure. The effects of fluid-structure interaction (FSI) caused by the passive containment cooling system water storage tank (PCCWST) on NPP's seismic performance are investigated. The FSI of water tank theoretical model is considered based on the Housner's model, and a series of time history analyses are performed to prove the rationality of the proposed model. Three single-objective optimization strategies are employed to minimize the relative displacement variance and absolute acceleration variance of the upper structure, as well as the filtered energy index (FEI). Furthermore, a multi-objective optimization strategy considering all these three indexes is proposed to obtain optimal parameters of vibration control. The influence of vibration control strategies on the relative deformation and acceleration of the upper structure is explored with various water level ratios. The analytical results indicate that the proposed BIS-TMDI strategy has significantly reduced the NPP structure's seismic response. The effectiveness of the vibration control strategy is influenced by the water level ratio, emphasizing the significance of designing an appropriate water level ratio to reduce NPP structure's seismic response.

1. Introduction

The nowadays main theme of social development revolves around the green economy, and nuclear energy is gaining prominence owing to its heightened efficiency and environmental advantages. The NPP structure, such as AP1000 NPP, primarily comprises five major parts, namely nuclear island facility, turbine hall, auxiliary buildings, diesel generator building, and radioactive waste facility. The nuclear island includes a steel containment structure, a shielding building (SB), and auxiliary facilities [1]. Due to the 2011 Tōhoku earthquake, an immeasurable impact on human health is continually worsen by the leakage of Fukushima NPP [2]. Earthquakes can cause a severe accident at NPP structures, and the seismic safety issue of NPP structure is a major concern to the communities in many countries.

Numerous investigations have been conducted to enhance the seismic safety of NPP structures. In regard to seismic vibration control strategies for NPP, isolators have been frequently positioned beneath the foundation to provide additional energy dissipation, which decrease the seismic response of the upper structures [3]. Surh et al. [4] implemented a BIS design in the advanced power reactor 1400 (APR1400), revealing a significant reduction in the primary stresses of the APR1400 structure under seismic loading. Frano and Forasassi [5] demonstrated that BIS strategy led to a reduction of the maximum horizontal acceleration response at the base of the reactor pressure vessel. Ostrovskaya and Rutman [6] explored the support-pendulum seismic isolation system (a type of BIS), illustrating a twofold reduction in the horizontal velocity and acceleration of the NPP's equipment. However, adopting BIS strategy alone may lead to excessive horizontal deformation of the isolation layer. The damping of isolation layers is designed to decrease the deformation of the isolation layer. However, the increased damping might lead to an increase of the structural acceleration [7], potentially having adverse effects on the NPP. Furthermore, the tuned mass dampers (TMD) system vibration control strategy could be used simultaneously to reduce structural seismic response. Frahm [8] first utilized the TMD to mitigate lateral rotation and oscillation of ship structures, and Taniguchi et al. [9] found that the implementation of a TMD on the

* Corresponding author.
E-mail address: caixuesongbest@hrbeu.edu.cn (X. Cai).

https://doi.org/10.1016/j.net.2024.02.019
Received 21 November 2023; Received in revised form 31 January 2024; Accepted 9 February 2024
Available online 16 February 2024
1738-5733/© 2024 Korean Nuclear Society. Published by Elsevier B.V. This is an open access article under the CC BY-NC-ND license (http://creativecommons.org/licenses/by-nc-nd/4.0/).

isolation layer resulted in a reduction of 15%–25% in the displacement of the base-isolated building. Azeem et al. [10] conducted parameter studies on seismic performance of structure equipped with TMD devices, demonstrating that an optimized TMD led to a decrease of the base displacement by 40% subjected to earthquake excitations of the Imperial Valley and Loma Prieta. Wang et al. [11] introduced a semi-active tuned mass damper (STMD) with variable stiffness and damping ratios to an eight-story structure. The analytical results indicated that the STMD effectively reduced the displacement and acceleration responses of both linear BIS and nonlinear BIS. Kwag et al. [12] proposed the TMD device to mitigate the seismic response of nuclear piping systems, showing that the application of the TMD reduced the average maximum acceleration response of the pipes by 34%. However, the anticipated mass ratio of the TMD is substantial, posing a challenge in practical design [13]. Hence, an inerter device was proposed by Smith [14] to enhance vibration suppression effects and amplify the mass ratio significantly. Marian and Giaralis [15] proposed a TMDI system connected to the ground, which was designed to effectively suppress the vibration of linear structural systems. Angelis et al. [16] proposed the BIS-TMDI strategy to reduce the lateral displacement demands of BIS structures. The results indicated that under all considered excitations, the adoption of a ground-connected inerter device could reduce secondary mass displacement, while also improve BIS displacement demands in most cases. Domenico and Ricciardi [17] compared the BIS-TMDI system with other vibration control systems, demonstrating that the BIS-TMDI system had several advantages, which reduced BIS displacement and upper structure response effectively without causing excessive stroke in the TMDI. Pietrosanti et al. [18] discussed the nonlinear TMDI vibration suppression deviating from the ideal linear inerter element through shaking table testing. The results indicated that the influence of the nonlinear properties of the inerter device on the displacement, acceleration, and base shear responses of a single-degree-of-freedom structure was not significant. Pietrosanti et al. [19] evaluated the potential of inerter vibration absorbers (IVA) in the BIS-TMDI structure through shaking table testing, considering the combined effects of nonlinear inerter and structural behavior. The results showed that with an increase in inertance and fixed secondary mass, IVA became more effective in mitigating BIS displacement and base shear response simultaneously. Bian et al. [20] applied the BIS-TMDI strategy to a high-voltage substation to enhance the seismic resistance of frame steel switches. The results revealed that the maximum displacement response of the frame was reduced by 40%. Therefore, the application of the BIS-TMDI in AP1000 NPP structure emerges as an alternative strategy to control their vibrations subjected to earthquake excitation.

As an integral component of the AP1000 NPP, the PCCWST is situated atop the SB. In emergency situations, the PCCWST ensures equipment safety by cooling the steel containment through gravity-driven water spray [21]. The water in the PCCWST of the AP1000 NPP has a significant impact on the seismic response of the NPP structure [22]. Jiang et al. [23] proposed an optimization design method based on a closed-form solution for liquid tanks with inerter isolation systems considering FSI effects. The reduction in sloshing height reached up to 85% compared to tank without vibration control system. Luo et al. [24] proposed a hybrid vibration control method for liquefied natural gas (LNG) storage tanks, using the series viscous mass damper (SVMD) devices and lead-core rubber bearings (LRB) together. The results indicated that SVMD could effectively control sloshing height, demonstrating favorable damping effects. Labaf et al. [25] employed a BIS-TMDI hybrid control system to suppress vibrations in steel storage tanks subjected to seismic excitation. Compared to the uncontrolled steel storage tanks, this system could reduce the convective and impulsive displacements as well as the base shear force by over 80%. Zhang et al. [26] introduced a friction pendulum inerter system to enhance the seismic performance of base-isolated tanks considering FSI effects. The results indicated that this system could effectively improve the seismic performance of the tank, particularly in terms of isolation displacements. Zhao et al. [27] employed the finite element method (FEM) to analyze the effects of various water levels of the PCCWST on seismic responses of NPP structure. The results indicated that the seismic performance of FEM models with various water levels distinguished considering FSI. Xu et al. [22] utilized both the smoothed particle hydrodynamics method and FEM to simulate FSI between the water and the AP1000 shield structure, showing that the structural fundamental frequency decreases with an increase of water level. Zhang et al. [28] constructed a scaled model of the AP1000 for shaking table test and conducted the FEM modeling of tested model using ABAQUS, affirming the dampening effect of PCCWST considering FSI. The presence of water in the PCCWST led to a reduction of approximately 5–20% in the peak acceleration, and a decrease of about 5–10% in the structural bottom strain. However, the BIS-TMDI hybrid vibration control strategy for the AP1000 NPP structure considering FSI effects are not clear. Meanwhile, investigations on simplified structural models of AP1000 NPP and its optimal parameter of vibration control remain limited.

This study aims to enhance the seismic performance of the AP1000 NPP by analyzing the structure equipped with a BIS-TMDI system, considering the FSI of the NPP water tank. The effects of various water level ratios of the PCCWST on the structural seismic performance is thoroughly studied. Meanwhile, the various optimization methods are applied to reduce the upper structure's displacement variance, the upper structure's absolute acceleration variance, and the filtered energy index (FEI). Furthermore, time history analyses are performed on the AP1000 NPP with various vibration control strategies subjected to the RG1.60 artificial wave excitation. The relative displacement between the upper and lower structures, as well as the acceleration of the upper structure are studied, considering different water level ratios and diverse vibration control strategies. This study presents a theoretical solution to reduce the seismic response of AP1000 NPP structure, which offers significant engineering value and design guidance.

2. AP1000 NPP simplified model and model validation

2.1. Theoretical model of the AP1000 NPP

The AP1000 NPP structure is shown in Fig. 1, including the steel containment structure, the SB, and the basemat of the support for the SB, as well as the PCCWST. The basemat is a cast-in-place reinforced concrete foundation with a thickness of 6.87 m, while the steel containment vessel reaches a height of 65.63 m. The height of the PCCWST is 11.80

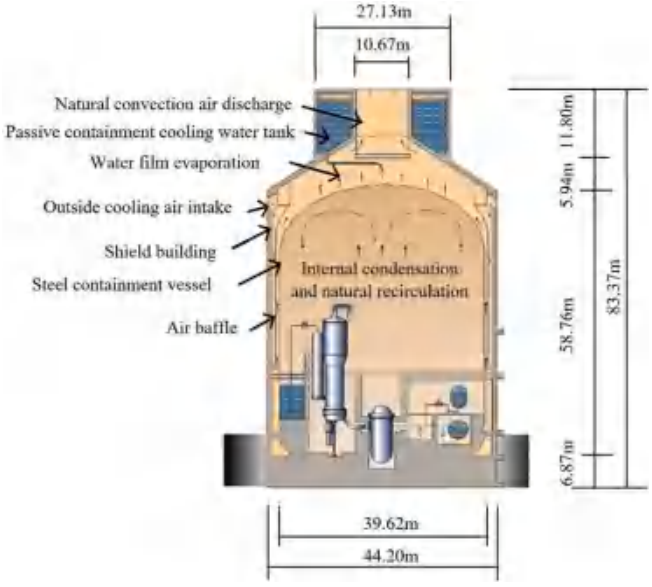

Fig. 1. Geometry of the SB and PCCWST [29].

m, and specific structural dimensions of the AP1000 are outlined in Table 1 [29]. The containment building situated on rigid soil is simplified as a mass-spring model with two degrees of freedom [30,31].

It is assumed that the water tank walls are rigid, the water exhibits negligible viscosity, and both the tank and water motions remain linearly elastic. Therefore, a simplified Housner's model is applied to simulate the FSI between the water and the PCCWST [32]. The water mass of the tank is split accordingly into impulsive mass and convective mass. The impulsive mass adhered to the tank moves along with PCCWST, while the convective mass is connected to the tank surface through spring elements. Because the water tank atop of the AP1000 containment building is not cylindrical, it is necessary to transform the PCCWST into a standard cylindrical shape. As depicted in Fig. 2, h represents the original water height of the tank maintaining a constant value, and R denotes the radius of the cylindrical water tank. The formulas for impulsive mass stiffness, convective mass stiffness, and the corresponding spring stiffness for convective motion are as follows [33].

$$m_0 = \begin{cases} M\dfrac{\tanh\left(\sqrt{3}R/h\right)}{\sqrt{3}R/h}, h < 1.5R \\ M(1\text{-}0.436R/h), h > 1.5R \end{cases} \tag{1}$$

$$m_1 = 0.455\frac{R}{h}\tanh\left(\sqrt{\frac{27}{8}}\ \frac{h}{R}\right)M \tag{2}$$

$$k_1 = m_1\sqrt{\frac{27}{8}}\ \frac{g}{R}\tanh\left(\sqrt{\frac{27}{8}}\ \frac{h}{R}\right) \tag{3}$$

Where M represents the water mass of the tank, m_0 denotes the impulsive mass, m_1 signifies the convective mass, and k_1 stands the stiffness for convective motion. Due to the fact that NPP structures are typically constructed on solid bedrock, soil-structure interaction (SSI) is not considered in this study [34–36]. The schematic representation of the AP1000 NPP structure with the integrated BIS-TMDI system is depicted in Fig. 3. m_b is considered as the mass of the lower structure including the mass of the basemat, and the lower portion both of the steel containment vessel and SB. m_s is named as the mass of the upper structure, which encompasses the mass of the upper portion including steel containment and SB. The m_{str} corresponds to the mass of the water tank. It is noted that the BIS includes mass m_b, stiffness k_b, and damping C_b. In this hybrid vibration control strategy, the TMDI subsystem is connected to the lower structure through a linear spring stiffness k_t and a dashpot viscous damping C_t. m_t stands for the inherent mass of the TMDI system, while b_t is the apparent mass associated with inertia. The inertial device contains an embedded ball screw, allowing it to generate substantial inertial forces with a relatively small physical mass, resulting in a significant increase in inertia [14,37]. It should be noted that the physical mass of the inerter device is negligible when compared to its inertance [38]. C_s, k_{str0}, and C_{str0} represent the stiffness and damping of the upper structure and the stiffness and damping of the water tank.

Table 1
Dimensions of SB, PCCWST, basemat, and steel containment vessel.

Component	Parameter	Value
SB	Out diameter (m)	44.20
	Inner diameter (m)	42.38
	Thickness (mm)	912.00
	Height (m)	83.37
PCCWST	Out diameter (m)	27.13
	Inner diameter (m)	10.67
	Thickness (mm)	600.00
	Height (m)	11.80
Basemat	Diameter (m)	44.20
	Height (m)	6.87
Steel containment vessel	Out diameter (m)	39.53
	Inner diameter (m)	39.44
	Thickness (mm)	45.00
	Height (m)	65.63

2.2. Equations of motion of the AP1000 NPP structure equipped with BIS-TMDI

The AP1000 NPP structure equipped with the BIS-TMDI is subjected to the horizontal ground acceleration $\ddot{U}_g$. U_1 represents the relative displacement of the convective mass concerning the ground, while both the water tank and the impulsive mass share the same relative ground displacement denoted as U_0. The variables U_s, U_b, and U_t correspond to the relative ground displacements of the upper structure, the lower structure, and the TMDI system. For simplicity, $U_{1s} = U_1 - U_0$, $U_{0s} = U_0 - U_s$, and $U_{sb} = U_s - U_0$ are introduced. D'Alembert's principle is applied to derive the equations of motion of the BIS-TMDI AP1000 NPP theoretical model as follows:

$$\boldsymbol{M}\ddot{U}(t) + \boldsymbol{C}\dot{U}(t) + \boldsymbol{K}U(t) = -\tau\ddot{U}_g(t) \tag{4}$$

The symbol '·' signifies the derivative with respect to time. $\boldsymbol{M}$, $\boldsymbol{C}$, and $\boldsymbol{K}$ represent the matrices of mass, damping, and stiffness, respectively.

$$\begin{aligned} \boldsymbol{M} &= \begin{bmatrix} \mu_1 & \mu_1 & \mu_1 & \mu_1 & 0 \\ 0 & \mu_{str0} & \mu_{str0} & \mu_{str0} & 0 \\ 0 & 0 & 1 & 1 & 0 \\ 0 & 0 & 0 & \mu_b & 0 \\ 0 & 0 & 0 & 0 & \mu_{et} \end{bmatrix}\boldsymbol{K} \\ &= \begin{bmatrix} \omega_1^2\mu_1 & 0 & 0 & 0 & 0 \\ -\omega_1^2\mu_1 & \omega_{str0}^2\mu_{str0} & 0 & 0 & 0 \\ 0 & -\omega_{str0}^2\mu_{str0} & \omega_s^2 & 0 & 0 \\ 0 & 0 & -\omega_s^2 & \omega_b^2\mu_b + \omega_t^2\mu_{et} & -\omega_t^2\mu_{et} \\ 0 & 0 & 0 & -\omega_t^2\mu_{et} & \omega_t^2\mu_{et} \end{bmatrix} \\ \boldsymbol{C} &= \begin{bmatrix} 0 & 0 & 0 & 0 & 0 \\ 0 & 2\zeta_{str0}\omega_{str0}\mu_{str0} & 0 & 0 & 0 \\ 0 & -2\zeta_{str0}\omega_{str0}\mu_{str0} & 2\zeta_s\omega_s & 0 & 0 \\ 0 & 0 & -2\zeta_s\omega_s & 2\zeta_t\omega_t\mu_{et} + 2\zeta_b\omega_b\mu_b & -2\zeta_t\omega_t\mu_{et} \\ 0 & 0 & 0 & -2\zeta_t\omega_t\mu_{et} & 2\zeta_t\omega_t\mu_{et} \end{bmatrix}\tau \\ &= \begin{bmatrix} \mu_1 \\ \mu_{str0} \\ 1 \\ \mu_b \\ \mu_t \end{bmatrix} \quad U(t) = \begin{bmatrix} U_{10} \\ U_{0s} \\ U_{sb} \\ U_b \\ U_t \end{bmatrix} \end{aligned} \tag{5}$$

The matrices $\boldsymbol{M}$, $\boldsymbol{C}$, $\boldsymbol{K}$, and τ obtained in the above results are all divided by m_s.

$$\begin{aligned} &\mu_1 = \frac{m_1}{m_s};\ \mu_{str0} = \frac{m_0 + m_{str}}{m_s};\ \mu_b = \frac{m_b}{m_s};\ \beta_t = \frac{b_t}{m_s};\ \mu_t = \frac{m_t}{m_s};\ \mu_{et} \\ &= \mu_t + \beta_t;\ m_{str0} = m_0 + m_{str} \end{aligned} \tag{6a}$$

$$\begin{aligned} &\omega_1 = \sqrt{\frac{k_1}{m_1}};\ \omega_{str0} = \sqrt{\frac{k_{str0}}{m_0 + m_{str}}};\ \omega_s = \sqrt{\frac{k_s}{m_s}};\ \omega_b = \sqrt{\frac{k_b}{m_b}};\ \omega_t \\ &= \sqrt{\frac{k_t}{m_t + b_t}};\ \nu_t = \frac{\omega_t}{\omega_b} \end{aligned} \tag{6b}$$

$$\zeta_{str0} = \frac{C_{str0}}{2\omega_{str0}(m_0 + m_{str0})};\ \zeta_s = \frac{C_s}{2\omega_s m_s};\ \zeta_b = \frac{C_b}{2\omega_b m_b};\ \zeta_t = \frac{C_t}{2\omega_t(m_b + b_t)} \tag{6c}$$

Where μ_1 and μ_b represent the ratios of convective mass m_1 and lower structure mass m_b to upper structure mass m_s, respectively. The impulsive mass is directly attached to the water tank and moves together with it. The impulsive mass and water tank mass are considered together, denoted as m_{str0}. In the TMDI system, the effective mass ratio is denoted

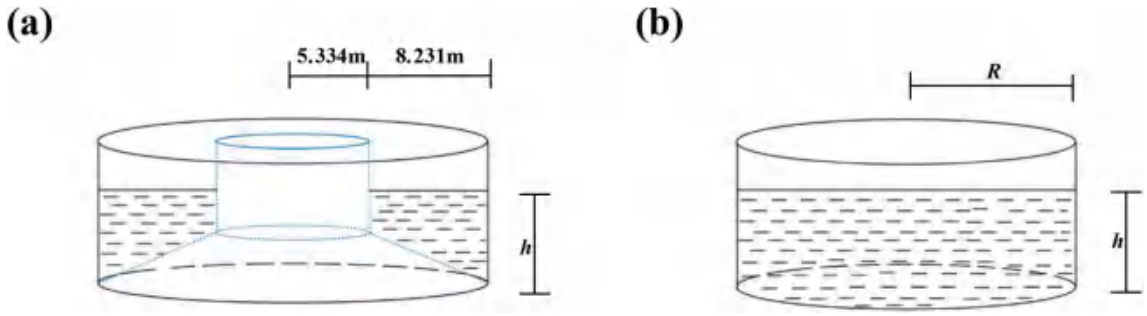

Fig. 2. Models of water tank: (a) PCCWST; (b) equivalent cylindrical water tank.

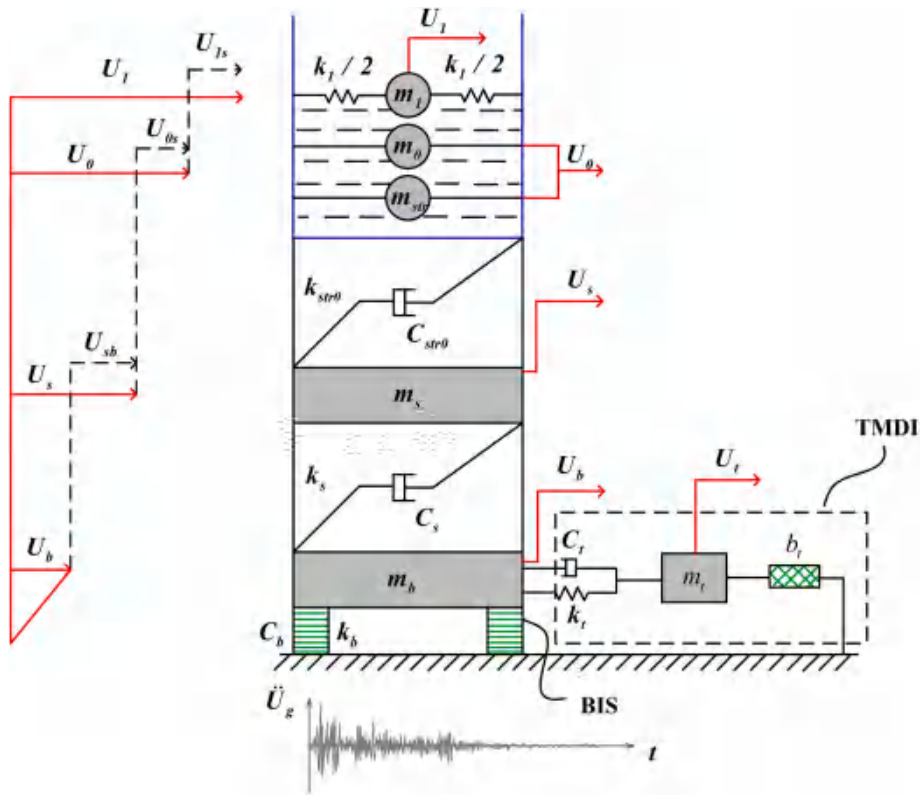

Fig. 3. Sketch of AP1000 NPP structure with the BIS-TMDI strategy.

as μ_{et}, μ_t is the ratio of inherent mass m_t to m_s, β_t represents the ratio of the apparent mass of the inerter device b_t to m_s, and β_t does not influence the magnitude of the seismic response of the NPP structure. When β_t is 0, the TMDI system is considered as an extension of the TMD system.

2.3. Seismic response of the AP1000 NPP theoretical model

The theoretical model of the AP1000 NPP equipped with the BIS-TMDI considering FSI effects is introduced in Section 2.2. To validate the rationality of the proposed model, time history analyses are performed on the theoretical model of the AP1000 without the BIS and TMDI strategies. The influence of water level ratio of the PCCWST on the response of the upper structure is investigated. Through modal analysis of the steel containment vessel and shield building of the AP1000 NPP in ANSYS [35], the fundamental frequencies of the structures were obtained, serving as the basis for determining theoretical model parameters: The fundamental frequency of the AP1000 NPP is 4.04 Hz, and the fundamental frequency of NPP structure with BIS strategy decreases to 0.30 Hz. The damping ratio of the BIS part is 10%, and the damping ratio of the upper structure is 5% ($\zeta_s = 0.05$, $\zeta_b = 0.10$). When the water level ratio is determined, the corresponding values of impulsive mass, convective mass, and stiffness associated with convective motion are obtained. Consequently, μ_1 , μ_{str0}, ω_1, ω_{str0}, and ζ_{str0} are determined with specific values at a certain height ratio, and ω_s is 28.06. The recorded El-Centro ground acceleration time history is employed in the seismic analyses of NPP structures [39,40]. A peak ground acceleration (PGA) of 0.3g El-Centro record is selected for time history analyses. Zhao et al. [27] modeled the AP1000 NPP structure using LS-DYNA and conducted time-history analysis. The El-Centro record was utilized in the north-south and east-west directions with a PGA of 0.5g, and the vertical PGA was set as 0.33g. Wang et al. [29] modeled the AP1000 NPP structure using ANSYS. The selected San Fernando earthquake wave closely matched the design standard spectrum of RG1.60. Time-history analysis was performed using the 0.3g San Fernando earthquake wave in the north-south and east-west directions, where the vertical PGA was set to 2/3 of the horizontal acceleration. In the outcomes of aforementioned models, the effects of different water level ratios on the maximum displacement and acceleration responses of the upper structure have been normalized, and the normalized results are presented in Fig. 4. H_w represents the height of the water tank, and h is the height of the water

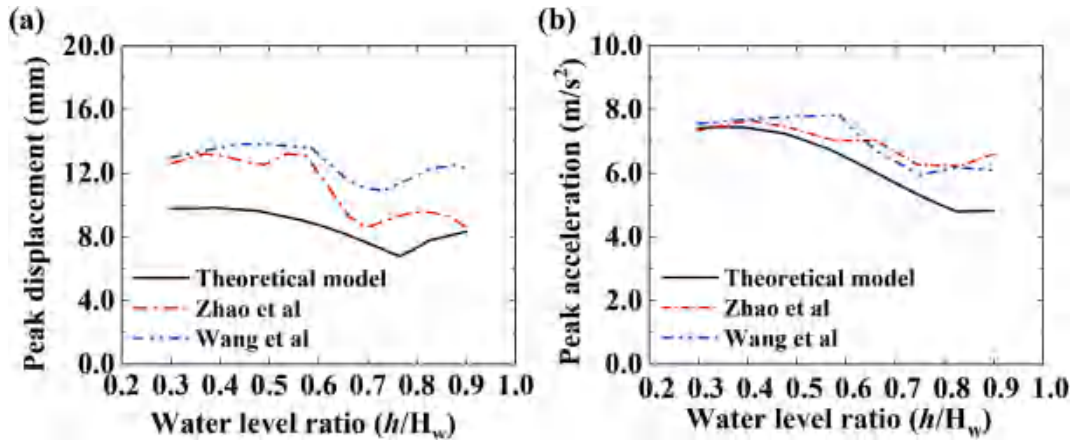

Fig. 4. The relationship between the response of the upper structure and the water surface height *h*: (a) Peak displacement; (b) peak acceleration.

surface. It is evident that water level ratio does not exhibit a monotonic relationship with the maximum displacement of the upper structure. All the three model outcomes indicate that with the increase in water level ratio, the maximum displacement of the upper structure initially shows a decreasing trend and reaches its minimum at a water level ratio of 0.7–0.8. Subsequently, the maximum displacement shows an increasing trend. The cause of this phenomenon is the varying vibration frequencies of the structure due to different water levels. The maximum acceleration of the upper structure reaches its minimum around a water level ratio of 0.8 in all the three models. The differences among the three curves in Fig. 4 are attributed to that the theoretical model adopts unidirectional horizontal seismic motion, while Wang et al.'s and Zhao et al.'s works utilized three-dimensional seismic motion. Additionally, variations in the input seismic waves also contribute to the slight discrepancy observed in the three curves. It is noted that the differences among the three curves are acceptable, and both the maximum displacement and maximum acceleration curves exhibit the same trend, which confirms the validity of the theoretical model.

3. Optimization strategy for the AP1000 NPP structure equipped with the BIS-TMDI

3.1. Determination of optimization problem parameters

The equations of motion of the simplified AP1000 NPP model equipped with a BIS-TMDI considering FSI effects are established. To reduce the seismic response of the AP1000 NPP structure at different water level ratios, it is necessary to perform parameter optimization on the structure equipped with the BIS-TMDI. In the AP1000 NPP theoretical model with the BIS-TMDI, the optimal frequency ratio ν_t and damping ratio ζ_t are identified with varying water level ratios (μ_b = 2.948, $\omega_s = 28.060$, and $\omega_b = 1.822$). The optimal combination (ν_t, ζ_t) to minimize the objective functions (OFs) of the structural system's dynamic response is achieved using **fmincon** function. The optimization variables are represented as $x = (\nu_t, \zeta_t)$, with lower bounds $x_{lb} = [0.10, 0.01]$ and upper bounds $x_{ub} = [5.00, 1.00]$. Section 3.2 introduces the covariance matrix related to the OFs, while the discussion on different optimization OFs is given in Section 3.3.

3.2. Stochastic dynamic analysis method

Due to the stochastic fundamental of seismic excitation, this study assumes that the base acceleration follows a stationary Gaussian zero-mean stochastic process. The one-sided PSD matrix for the system displacement response $G_{uu}(\omega)$ is defined as follows:

$$G_{uu}(\omega) = H(\omega)\tau G_{\ddot{u}_g}(\omega)\tau^T H(\omega)^{*T} \tag{7}$$

Where $H(\omega)$ represents the frequency response function, and the relation between the covariance matrix $\sum_{UU}$ of the displacement response and the one-sided PSD matrix $G_{uu}(\omega)$ of the system displacement response is as follows [17]:

$$\sum_{UU} = \int_0^\infty G_{uu}(\omega)d\omega \tag{8}$$

The one-sided PSD matrix of the system's velocity response is denoted as $G_{\dot{u}\dot{u}}(\omega) = \omega^2 G_{uu}(\omega)$, and its velocity covariance matrix $\sum_{\dot{U}\dot{U}}$ is given by:

$$\sum_{\dot{U}\dot{U}} = \int_0^\infty G_{\dot{u}\dot{u}}(\omega)d\omega \tag{9}$$

3.3. Selection of the OFs

3.3.1. Variance of relative displacement of the upper structure, $OF_1 = \sigma^2_{U_s}$

By reducing the displacement variance of the upper structure, the structural integrity and safety could be enhanced, lowering the damage and fatigue levels of the NPP structure and extending the structural lifespan. In the case of an AP1000 NPP structure with the TMDI strategy, the relative displacement variance of the upper structure is denoted as $\sigma^2_{U_{s0}}$. The optimization effect of the relative displacement variance of the upper structure is considered under three conditions, namely when the water level ratios are 0, 0.5, and 0.9. Through the optimal parameter combination $x_{opt} = (\nu_{topt}, \zeta_{topt})$, the minimum displacement variance $\sigma^2_{U_s}$ of the upper structure is obtained with the hybrid BIS-TMDI vibration control strategy. The effectiveness of reducing the relative displacement variance of the upper structure with the BIS-TMDI strategy is measured using F_{1min}. When F_{1min} is less than 1.0, the BIS-TMDI strategy is beneficial to mitigate the relative displacement variance of the AP1000 NPP's upper structure. The optimization results are presented in Figs. 5–7, where each curve corresponds to a specific value of μ_t (0.01, 0.05, 0.1, 0.2, and 0.5).

$$F_{1min} = \frac{\sigma^2_{U_s}}{\sigma^2_{U_{s0}}} \tag{10}$$

It is seen in Figs. 5–7 that the variance of the upper structure's displacement decreases with the increasing β_t of the BIS-TMDI NPP structure. This indicates that the BIS-TMDI system is superior to the BIS-TMD system (β_t = 0) in mitigating the displacement variance of the upper structure. As β_t grows from 0 to 0.6, F_{1min} experiences an initial sharp decrease, followed by a more gradual decline. Generally, a larger value of μ_t leads to a reduced displacement variance of upper structure, but the differences in the variance influenced by varying μ_t gradually diminish with the increasing β_t. Overall, the optimal frequency ratio ν_{topt}

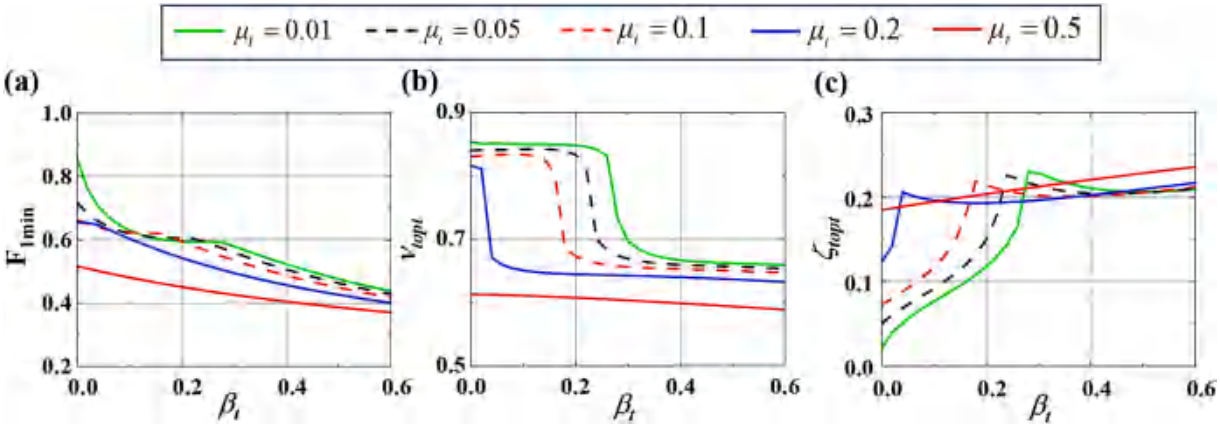

Fig. 5. When $h/H_w = 0.9$, the optimization result of the variance of relative displacement: (a) Minimum value of F_{1min}; (b) optimal frequency ratio; (c) optimal damping ratio.

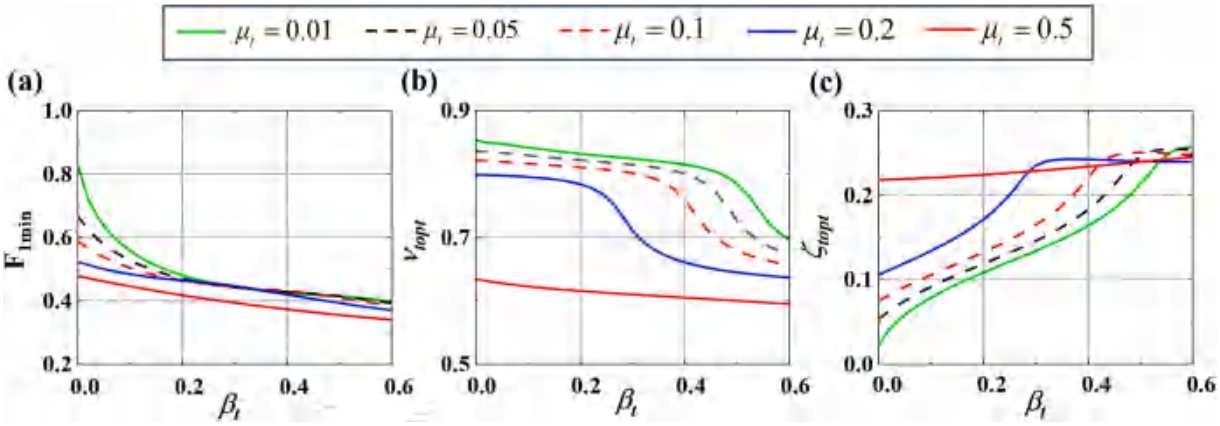

Fig. 6. When $h/H_w = 0.5$, the optimization result of the variance of relative displacement.

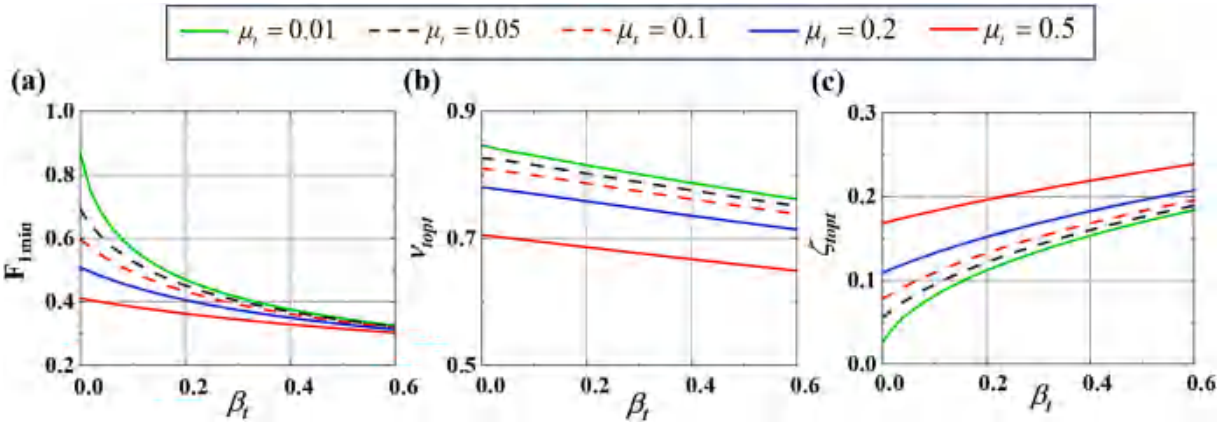

Fig. 7. When $h/H_w = 0$, the optimization result of the variance of relative displacement.

and damping ratio ζ_{topt} exhibit opposite trends. Specifically, the optimal frequency ratio ν_{topt} decreases as β_t increases, while the optimal damping ratio ζ_{topt} increases as β_t increases. When the water level ratio is 0, the higher values of μ_t correspond to the lower values of ν_{topt} and the higher values of ζ_{topt} for the same value of β_t. As the water level ratio decreases, the reduction in upper structure's displacement variance becomes more effective with the BIS-TMDI strategy. This is attributed to the more severe swaying and vibrating effects due to a relatively high water level ratio [27], which has an adverse impact on reducing F_{1min}. When $h/H_w = 0.9$, Fig. 5(b) and (c) demonstrate that there is a sudden change in the optimal frequency ratio ν_{topt} and optimal damping ratio ζ_{topt}, concerning variations in β_t with a relatively low value of μ_t. This phenomenon is influenced by the mass of water and the inherent mass of the TMDI system.

3.3.2. *Variance of absolute acceleration of the upper structure, $OF_2 = \sigma^2_{\ddot{U}_{stot}}$*

The absolute acceleration of upper structure is denoted as $\ddot{U}_{stot} = \ddot{U}_s + \ddot{U}_g$. Mitigating the absolute acceleration variance of the upper

structure is beneficial to diminish structural vibrations, ultimately enhancing the safety and reliability of the AP1000 NPP structure. F_{2min} is the ratio of absolute acceleration variance ($\sigma^2_{\ddot{U}_{stot}}$) of the AP1000 NPP equipped with BIS-TMDI to absolute acceleration variance ($\sigma^2_{\ddot{U}_{0stot}}$) of BIS AP1000 NPP and it serves as a gauge for evaluating the vibrational control efficacy of the BIS-TMDI system. When F_{2min} is less than 1.0, the BIS-TMDI strategy plays a positive role in reducing the seismic response of the AP1000 NPP, as illustrated in Figs. 8–10.

$$F_{2min}=\frac{\sigma^2_{\ddot{U}_{stot}}}{\sigma^2_{\ddot{U}_{0stot}}} \tag{11}$$

It is evident that the BIS-TMDI strategy is more beneficial to reduce the absolute acceleration of the NPP's upper structure, compared with the decreased relative displacement variance. When the water level ratio reaches 0.9, F_{1min} decreases by 30.5% and F_{2min} decreases by 41.9% on the condition that μ_t is 0.01 and β_t varies from 0 to 0.2. When the water level ratio of the tank is relatively low, the optimal frequency ratio ν_{topt} remains relatively stable as β_t changes, while the optimal damping ratio ζ_{topt} increases with the growth of β_t. It is noteworthy the change in F_{2min} is not very pronounced as the water level ratio decreases, when other parameters remain constant.

3.3.3. *FEI, OF_3 = FEI = 1-EDI*

The energy dissipation index (EDI) is applied to assess the stability and safety of a structure by analyzing the energy transfer and dissipation [17]. When a vibration control system absorbs the total energy input as effectively as possible, the optimal level of vibration reduction is achieved [41]. This study utilizes FEI as a seismic evaluation indicator, which focuses on enhancing the performance of the TMDI to reduce the energy input into the structure. The decreased FEI signifies a more effective utilization of the TMDI in the AP1000 NPP structure equipped with the BIS-TMDI system. By searching for the optimal frequency ratio ν_{topt} and damping ratio ζ_{topt}, the minimum FEI (FEI = 1-EDI) results are shown in Figs. 11–13. The following equations are derived from the structural analysis of Fig. 3.

$$\begin{cases} m_1\ddot{U}_1 = -m_1\ddot{U}_g - f_{t1} \\ (m_0+m_{str})\ddot{U}_0 = -(m_0+m_{str})\ddot{U}_g - f_{t2} + f_{t1} \\ m_s\ddot{U}_s = -m_s\ddot{U}_g - f_{t3} + f_{t2} \\ m_b\ddot{U}_b = -m_b\ddot{U}_g + f_{t3} + f_{t4} - f_{t5} \\ (m_t + b_t)\ddot{U}_t = -m_t\ddot{U}_g - f_{t4} \end{cases} \tag{12}$$

$$\begin{cases} f_{t1} = k_1U_{10} \\ f_{t2} = k_{str0}U_{0s} + C_{str0}\dot{U}_{0s} \\ f_{t3} = k_sU_{sb} + C_s\dot{U}_{sb} \\ f_{t4} = (U_t\text{-}U_b)k_t + (\dot{U}_t\text{-}\dot{U}_b)C_t \\ f_{t5} = U_bk_b + \dot{U}_bC_b \end{cases} \tag{13}$$

For Eq. (10), multiply both sides by $\dot{U}_1$, $\dot{U}_0$, $\dot{U}_s$, $\dot{U}_b$, and, $\dot{U}_t$ then,

$$\begin{cases} E_{k_1}(t) = E_{i_1}(t) - E_{e_1}(t) - E_{f_{t1}}(t) \\ E_{K_{str0}}(t) = E_{i_{str0}}(t) - E_{d_{str0}}(t) - E_{e_{str0}}(t) - E_{f_{t2}}(t) + E_{f_{t1}}(t) \\ E_{K_s}(t) = E_{i_s}(t) - E_{d_s}(t) - E_{e_s}(t) - E_{f_{t3}}(t) + E_{f_{t2}}(t) \\ E_{K_b}(t) = E_{i_b}(t) + E_{f_{t3}}(t) + E_{f_{t4}}(t) - E_{d_b}(t) - E_{e_b}(t) \\ E_{K_t}(t) = E_{i_t}(t) - E_{d_t}(t) - E_{e_t}(t) - E_{f_{t4}}(t) \end{cases} \tag{14}$$

Where $E_k(t)$, $E_i(t)$, $E_d(t)$, and $E_e(t)$ are the relative kinetic energy, relative input energy, viscous damping dissipation energy, and elastic strain energy, respectively. According to the law of conservation of mechanical energy, it is inferred that $E_k(t) + E_e(t) = 0$. $E_{f_{t1}}(t)$, $E_{f_{t2}}(t)$, $E_{f_{t3}}(t)$, and $E_{f_{t4}}(t)$ denote different aspects of energy transfer: the tank's inherent mass portion from convective motion, the upper structure from the tank's inherent mass portion, the lower structure from the upper structure, and the lower structure from the TMDI system. Within the time increment Δt, the following equations are obtained,

$$\begin{aligned} &\mathrm{E}[\Delta E_{i_1}] + \mathrm{E}\left[\Delta E_{i_{str0}}\right] + \mathrm{E}[\Delta E_{i_s}] + \mathrm{E}\left[\Delta E_{i_b}\right] + \mathrm{E}[\Delta E_{i_t}] \\ &= \mathrm{E}\left[\Delta E_{d_{str0}}\right] + \mathrm{E}[\Delta E_{d_s}] + \mathrm{E}\left[\Delta E_{d_b}\right] + \mathrm{E}[\Delta E_{d_t}] \end{aligned} \tag{15}$$

$$\begin{aligned} \mathrm{EDI} &= \frac{\mathrm{E}[\Delta E_{d_t}]}{\mathrm{E}[\Delta E_{i_1}] + \mathrm{E}\left[\Delta E_{i_{str0}}\right] + \mathrm{E}[\Delta E_{i_s}] + \mathrm{E}\left[\Delta E_{i_b}\right] + \mathrm{E}[\Delta E_{i_t}]} \\ &= \frac{\mathrm{E}[\Delta E_{d_t}]}{\mathrm{E}\left[\Delta E_{d_{str0}}\right] + \mathrm{E}[\Delta E_{d_s}] + \mathrm{E}\left[\Delta E_{d_b}\right] + \mathrm{E}[\Delta E_{d_t}]} \end{aligned} \tag{16}$$

$$\begin{aligned} \mathrm{FEI} &= 1\text{-EDI} \\ &= 1 - \frac{2\zeta_t\omega_t\mu_{et}\left(\sigma^2_{\dot{U}_t} + \sigma^2_{\dot{U}_b} - 2\sigma_{\dot{U}_t\dot{U}_b}\right)}{2\zeta_{str0}\omega_{str0}\mu_{str0}\sigma^2_{\dot{U}_{0s}} + 2\zeta_s\omega_s\sigma^2_{\dot{U}_{sb}} + 2\zeta_b\omega_b\sigma^2_{\dot{U}_b} + 2\zeta_t\omega_t\mu_{et}\left(\sigma^2_{\dot{U}_t} + \sigma^2_{\dot{U}_b} - 2\sigma_{\dot{U}_t\dot{U}_b}\right)} \end{aligned} \tag{17}$$

In the case where the water level ratio is 0, the optimal frequency ratio ν_{topt} exhibits a monotonically decreasing trend with the increasing β_t, while the optimal damping ratio ζ_{topt} demonstrates a monotonically increasing trend with the increasing β_t. As β_t changes from 0 to 0.6, there is no abrupt phenomenon observed in the variations of both the optimal frequency ratio ν_{topt} and optimal damping ratio ζ_{topt} on the condition that the water level ratio is 0. Overall, the FEI decreases with the reduction of water level ratio. Meanwhile, it is seen that FEI decreases with the in-

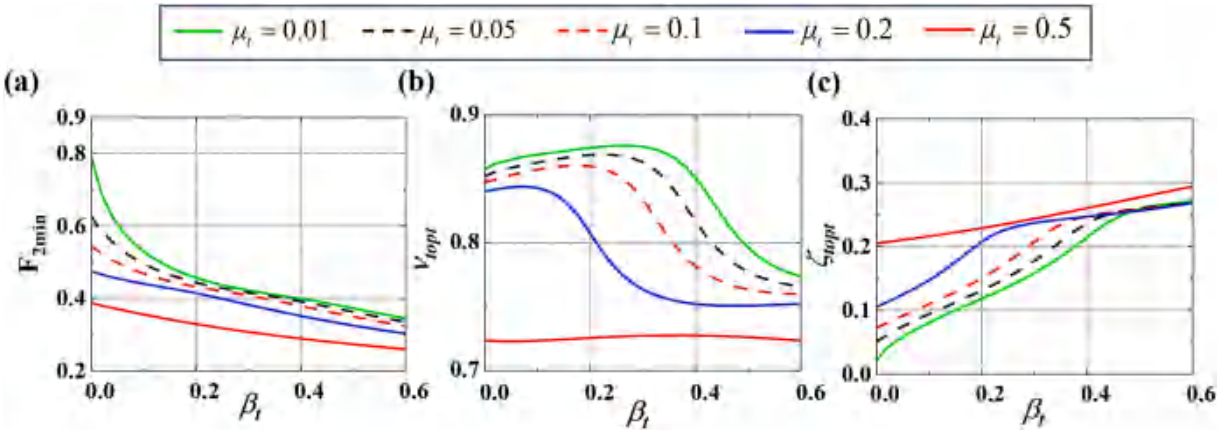

Fig. 8. When $h/H_w = 0.9$, the optimization result of the upper structure's absolute acceleration variance: (a) Minimum value of F_{2min}; (b) optimal frequency ratio; (c) optimal damping ratio.

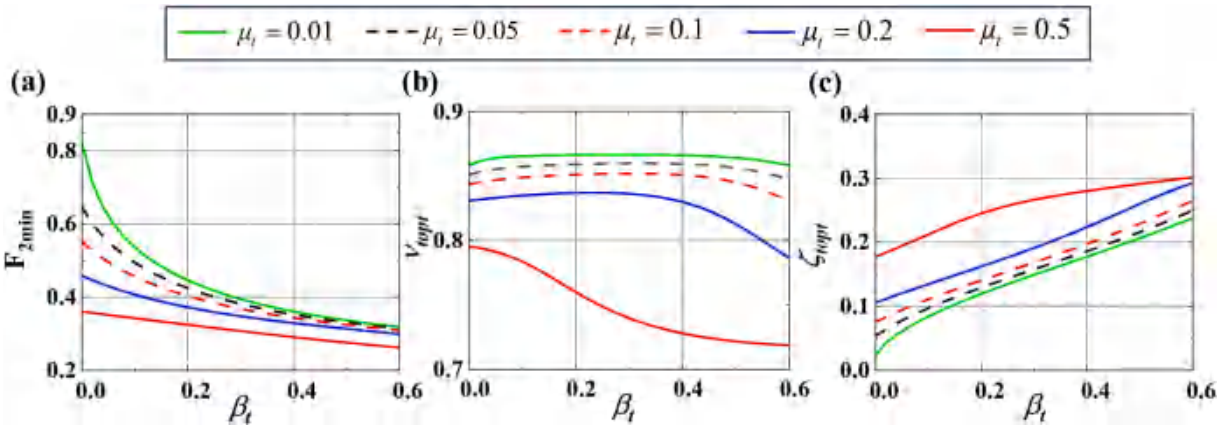

Fig. 9. When $h/H_w = 0.5$, the optimization result of the upper structure's absolute acceleration variance: (a) Minimum value of F_{2min}; (b) optimal frequency ratio; (c) optimal damping ratio.

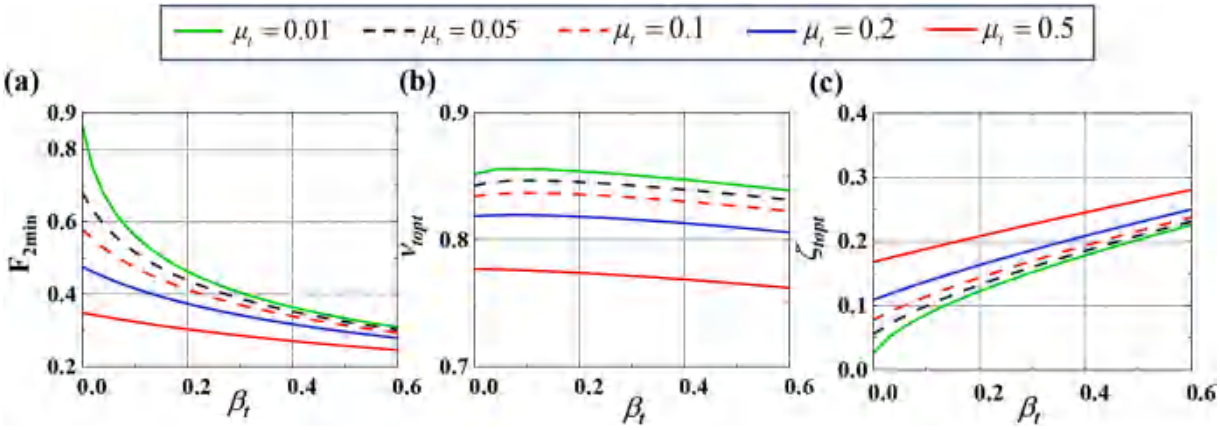

Fig. 10. When $h/H_w = 0$, the optimization result of the upper structure's absolute acceleration variance: (a) Minimum value of F_{2min}; (b) optimal frequency ratio; (c) optimal damping ratio.

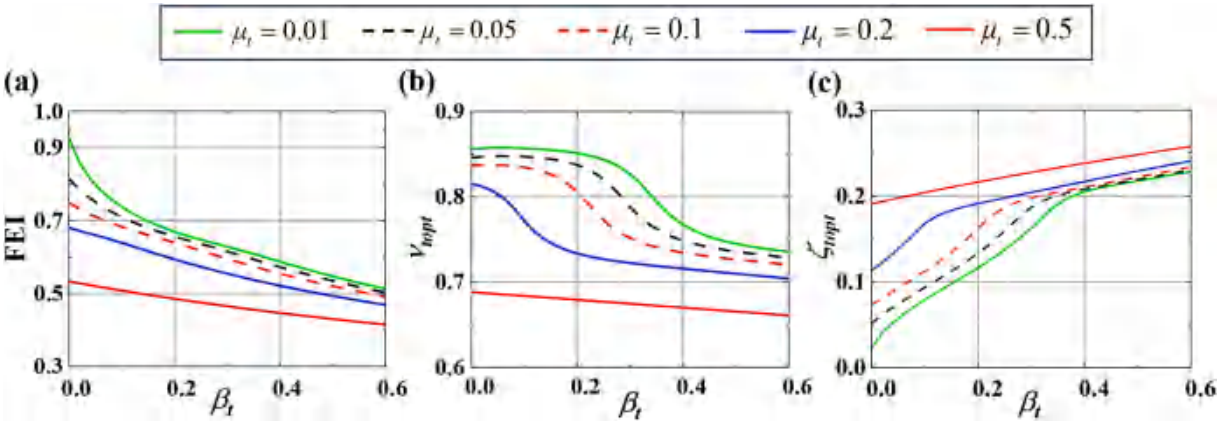

Fig. 11. When $h/H_w = 0.9$, the optimization result of the FEI: (a) Minimum value of FEI; (b) optimal frequency ratio; (c) optimal damping ratio.

crease value of μ_t when the water level ratio remains constant.

3.3.4. *Multi-objective optimization design, $OF_4 = F_{1min} + F_{2min} +$ FEI*

Based on the three above-mentioned single-objective optimization strategies, both the corresponding optimal frequency ratio ν_{topt} and optimal damping ratio ζ_{topt} are obtained when μ_t and β_t are predetermined. However, in practical engineering, it is challenging to achieve a relatively larger value of μ_t. Considering the AP1000 NPP structure, a choice of $\mu_t = 0.01$ and $\beta_t = 0.30$ is made for multi-objective optimization. By obtaining the optimal damping ratio ζ_{topt} and frequency ratio ν_{topt}, the total values of F_{1min}, F_{2min}, and FEI are minimized, denoted as OF_4. This choice ensures that the upper structure's displacement variance $\sigma^2_{\ddot{U}_s}$, the upper structure's absolute acceleration variance $\sigma^2_{\ddot{U}_{stot}}$, and the FEI are all chosen as favorable values. The results of multi-objective optimization of water level ratios of 0, 0.5, and 0.9 are shown in Figs. 14–16. In Fig. 14(a), F_{1min}, F_{2min}, and FEI are presented in

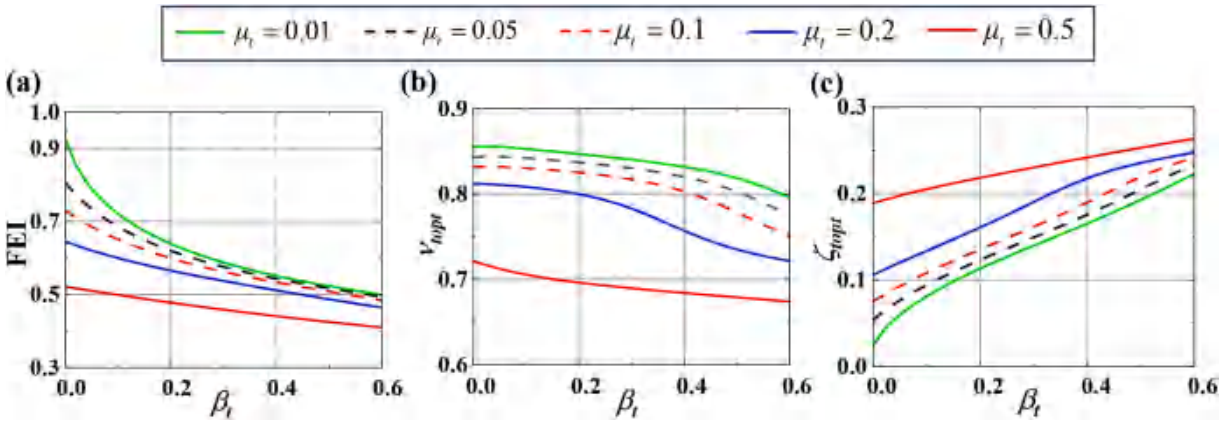

Fig. 12. When $h/H_w = 0.5$, the optimization result of the FEI: (a) Minimum value of FEI.

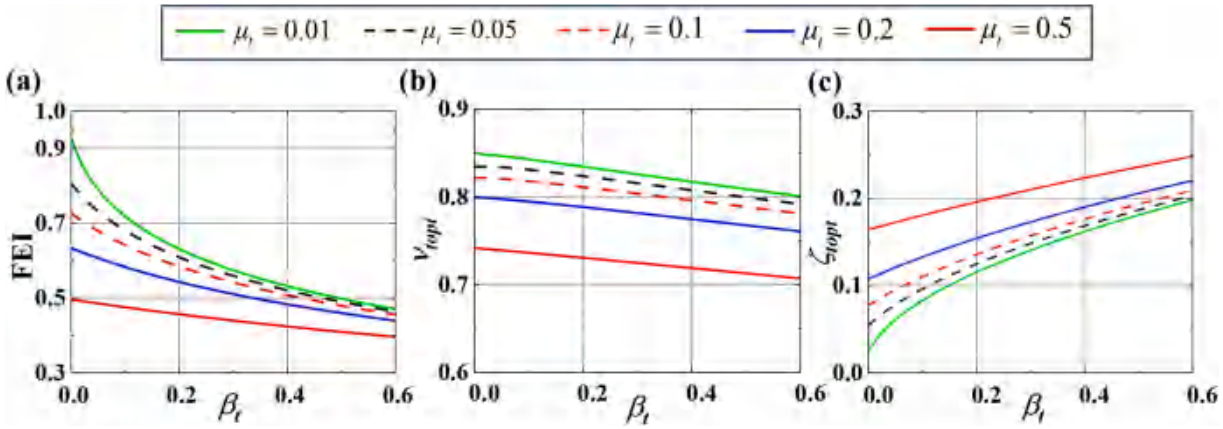

Fig. 13. When $h/H_w = 0$, the optimization results of the FEI: (a) Minimum value of FEI.

a three-dimensional way. In Fig. 14(b), the black dot represents the optimal performance point, which attains the best level of vibration reduction based on OF_4. Fig. 14(c) and (d) show the optimal frequency ratio ν_{topt} and the optimal damping ratio ζ_{topt}, corresponding to the best performance point. As shown in Table 2, before the water level ratio reaches 0.6, F_{1min} shows an increasing trend with the increase in water level ratio with slight fluctuations. As the water level continues to increase, F_{1min} sharply increases to 0.676 at a water level ratio of 0.7, followed by a decreasing trend. Although the trend of F_{2min} with the change in water level ratio is similar to F_{1min}, the overall variation is relatively smoother compared to F_{1min}. Before a water level ratio of 0.7, FEI generally shows an increasing trend with the increase in water level ratio. However, FEI exhibits a decreasing trend when the water level ratio ranges from 0.7 to 0.9. This phenomenon is related to the more severe swaying of the water as the water level increases, leading to a reduction in the energy dissipated by the TMDI relative to the input system. Simultaneously, it is closely associated with the fundamental frequency change of the AP1000 NPP structure due to different water level ratios. Through the above sensitivity analysis of seismic performance of NPP structures, setting the water level ratio around 0.6 is a practical strategy, considering that sufficient water is required in the AP1000 NPP's water tank for emergency.

4. Time history analysis of BIS-TMDI AP1000 considering FSI effects

In the above-mentioned analysis, a stationary white noise process is selected as the input to achieve the optimal performance of the TMDI. The optimal frequency ratio ν_{topt} and the optimal damping ratio ζ_{topt} are derived for different OFs. Basically, the white noise is a form of random vibrational model characterized by a flat frequency spectrum. As a matter of fact, real seismic motions exhibit clear temporal patterns. Hence, based on the design response spectrum of RG1.60 [42], an artificial wave (RG1.60) was generated using the **Seismoartif** [43] software with a PGA of 0.3g, ensuring that its response spectrum matches the design spectrum of RG1.60, as shown in Fig. 17.

The effectiveness of the proposed hybrid vibration control strategy is assessed by introducing the RG1.60 artificial wave to the AP1000 NPP structure equipped with the BIS-TMDI system. The relative displacement and the acceleration of the upper structure are compared among three models, namely fixed base (FB) NPP structure, BIS NPP structure, and BIS-TMDI NPP structure. In the AP1000 NPP structure equipped with the BIS-TMDI system, the values of the frequency ratio ν_t and damping ratio β_t are determined based on the optimal values obtained through multi-objective optimization with different water level ratios ($\mu_t = 0.01$ and $\beta_t = 0.30$). Fig. 18 depicts that the relative displacement of the upper structure with different water level ratios. The three curves represent three NPP structures with different strategies. It is evident that the FB AP1000 NPP structure presents the most severe seismic responses. Meanwhile, the NPP structure with BIS-TMDI strategy demonstrates superior seismic performance than that of the other two strategies. Specifically, the BIS system is able to provide appropriate damping to dissipate structural vibrations caused by earthquake excitations. Meanwhile, the TMDI system is capable of further suppressing the relative displacement, which is a key advantage of the BIS-TMDI strategy. As seen in Fig. 18(a-c), the reduction effects of relative displacement are greatest when the TMDI is introduced to the BIS NPP structure at a water level ratio of 0, compared with that of the other two

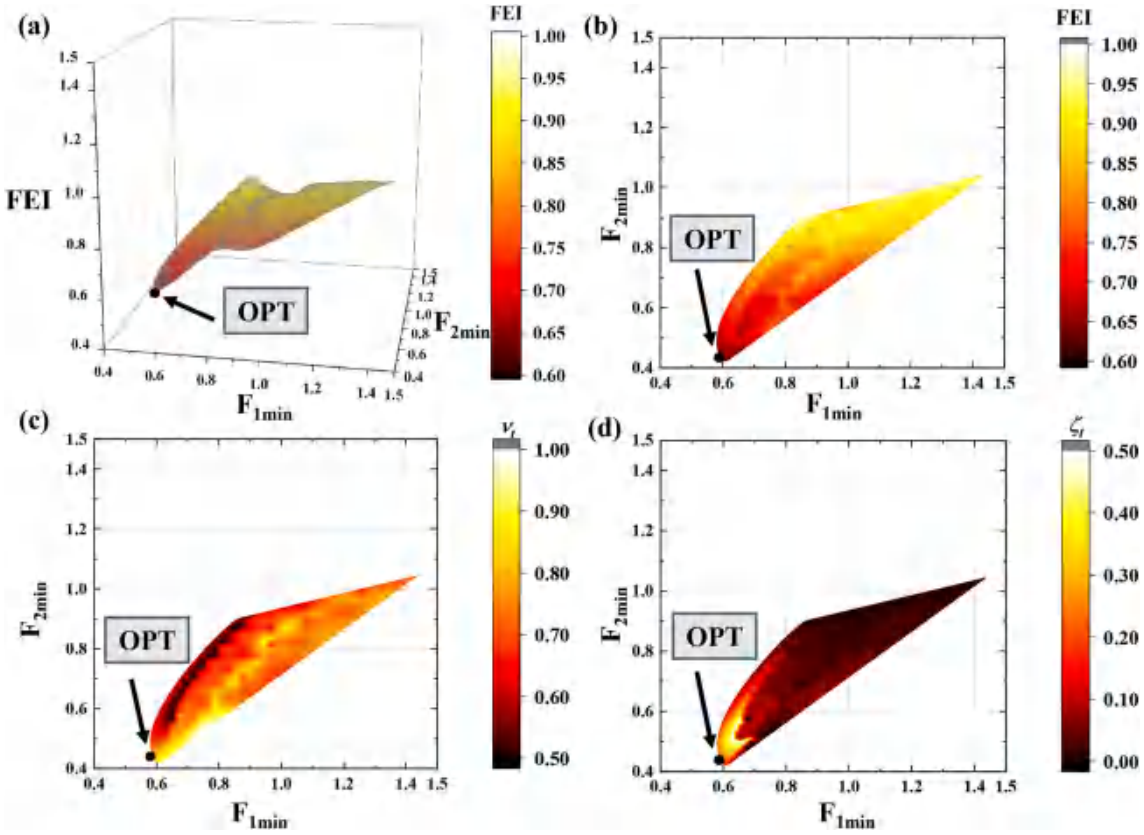

Fig. 14. Performance chart of multi-objective optimization, $h/H_w = 0.9$.

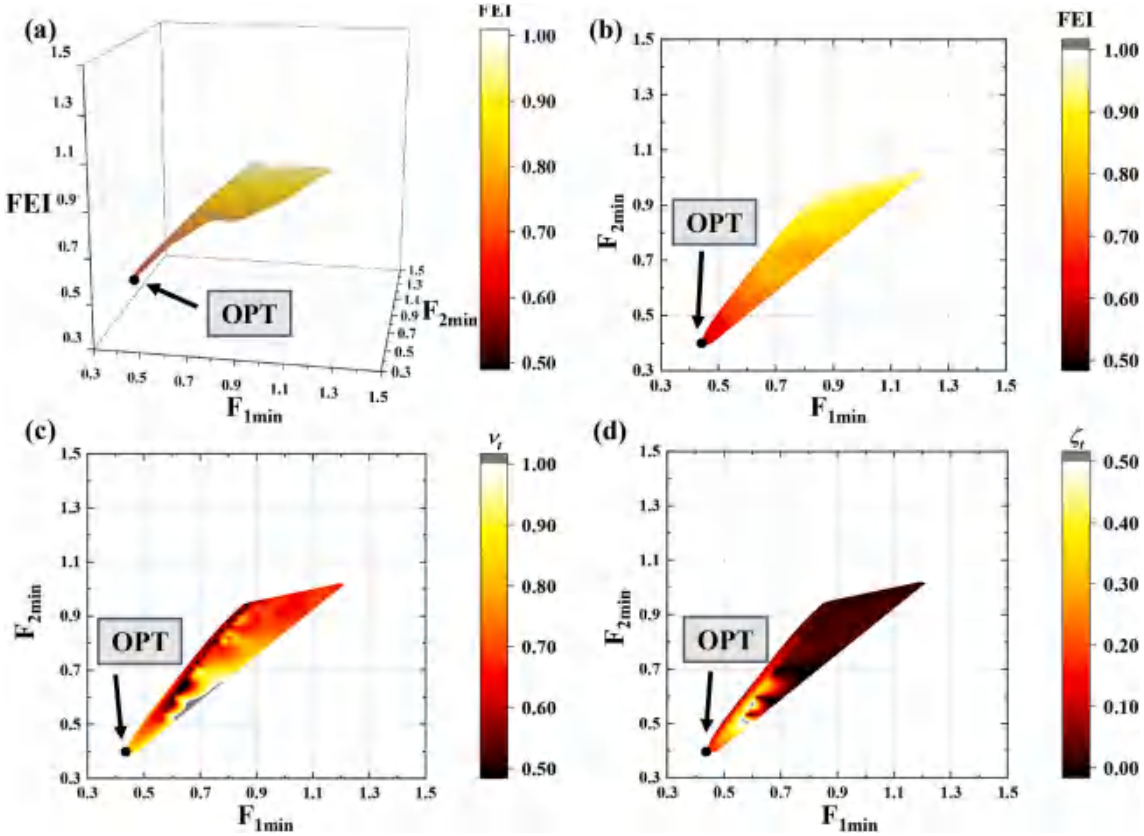

Fig. 15. Performance chart of multi-objective optimization, $h/H_w = 0.5$.

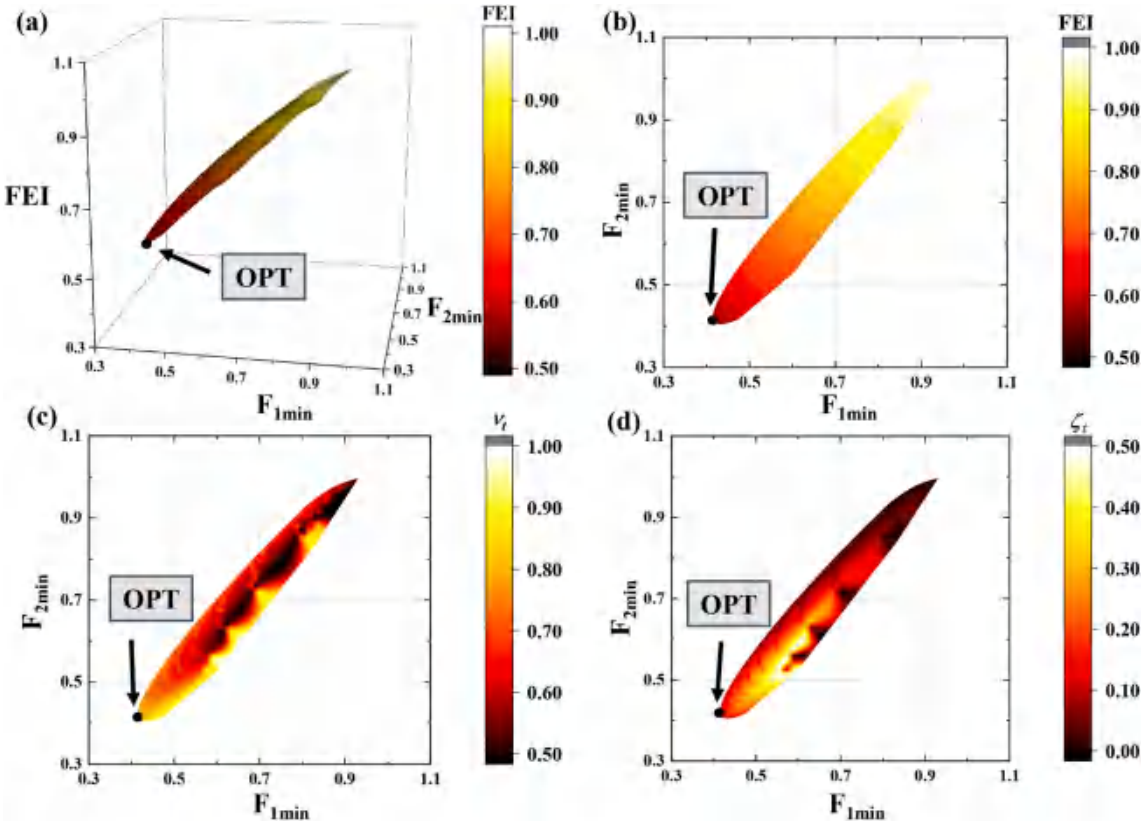

Fig. 16. Performance chart of multi-objective optimization, $h/H_w = 0$.

Table 2
The optimal parameters of BIS-TMDI AP1000 NPP structure with various water level ratios ($\mu_t = 0.01$ and $\beta_t = 0.30$).

Water level ratios : h/H_w	optimal frequency ratio: ν_{topt}	optimal damping ratio: ζ_{topt}	F_{1min}	F_{2min}	FEI
0	0.824	0.143	0.419	0.409	0.574
0.1	0.825	0.143	0.413	0.406	0.572
0.2	0.828	0.143	0.426	0.409	0.577
0.3	0.831	0.142	0.424	0.408	0.575
0.4	0.835	0.140	0.416	0.392	0.575
0.5	0.842	0.142	0.446	0.398	0.588
0.6	0.842	0.142	0.452	0.401	0.589
0.7	0.690	0.169	0.676	0.552	0.659
0.8	0.744	0.224	0.633	0.486	0.645
0.9	0.839	0.174	0.594	0.426	0.629

water level ratios. At varying water level ratios, the acceleration response spectrum of upper structures with different vibration control strategies, as well as the RG1.60 spectrum are depicted in Fig. 19. It is obvious that the upper structure's maximum spectral acceleration of the FB system is significantly larger than that of the AP1000 NPP structure employing the BIS and BIS-TMDI strategies. At water level ratios of 0, 0.5, and 0.9, the maximum spectral accelerations of the FB model are 49.75 m/s^2, 36.50 m/s^2, and 33.87 m/s^2, respectively. As the fundamental frequency of FB AP1000 NPP structure is 4.04 Hz (0.25 s), while the main frequency band of the RG1.60 artificial wave is within [0 s, 0.5 s]. This resonance induces amplification of the structural response. Conversely, with the implementation of the BIS and BIS-TMDI strategies, the inherent frequency of the AP1000 NPP structure is lowered, which avoids resonance and excessive vibration in alignment with the main frequency band of the RG1.60 artificial wave. Meanwhile, the peaks of the spectral accelerations with all three strategies are situated within the [0 s, 0.5 s] frequency band, because the energy of the RG1.60 artificial wave concentrates in this frequency range. It is evident that among the three vibration control strategies, the BIS-TMDI vibration control strategy results in the minimum acceleration response of the upper structure of the AP1000 NPP. Furthermore, the acceleration response spectrum curve of BIS-TMDI strategy closely approximates the RG1.60 design standard spectrum. In the frequency band [0 s, 3.3 s], there is minimal difference in the acceleration response spectrum curves of the upper structure between BIS and BIS-TMDI strategies. However, in the frequency band [3.3 s, 4.0 s], the BIS-TMDI strategy exhibits an excellent advantage over BIS strategy on vibration control of NPP structures.

Notably, in comparison with a water level ratio of 0, the acceleration response of the upper structure significantly decreases at water level ratios of 0.5 and 0.9. The cooling water of the PCCWST changes the structural fundamental frequency and mitigates the risk of excessive resonance. Consequently, it is evident that the appropriate cooling water in the PCCWST is advantageous for enhancing the vibration control effectiveness of the AP1000 NPP. In order to get a better understanding on the vibration control efficacy of the BIS and BIS-TMDI strategies, both the maximum relative displacement between the upper and lower structures, and the maximum acceleration of the upper structure under varying water level ratios are compared, as illustrated in Figs. 20-21. As seen in Fig. 20, the vibration control effect of the BIS-TMDI strategy on the maximum relative displacement is markedly superior to the BIS system. When the water level ratio is 0.1, the BIS-TMDI system shows an optimization of 25.45% in the maximum relative displacement compared with that of the BIS system. Even at a water level ratio of 0.7, an optimization of 12.16% is achieved, showing a significant vibration control effect on the BIS-TMDI AP1000 NPP structure. When adopting the BIS strategy, the maximum relative displacement between the upper and lower structures shows an initial decrease trend followed by an increase trend. However, an additional phase of decrease is observed in the AP1000 NPP structure with the BIS-TMDI strategy. This phenomenon is caused by the change of the structural inherent frequency induced

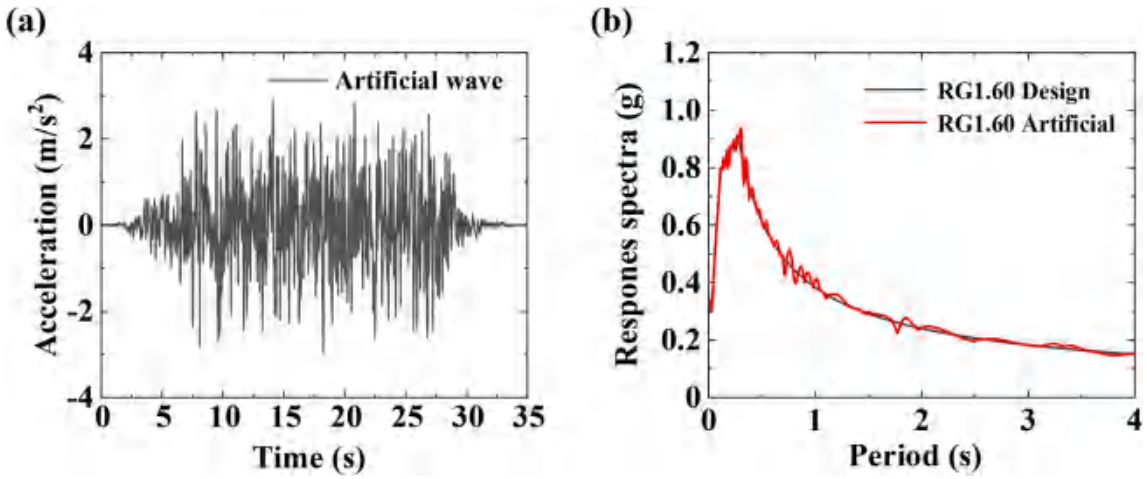

Fig. 17. The artificial wave and response spectrum of RG1.60:(a) RG1.60 artificial wave (b) design and artificial response spectrum of RG1.60.

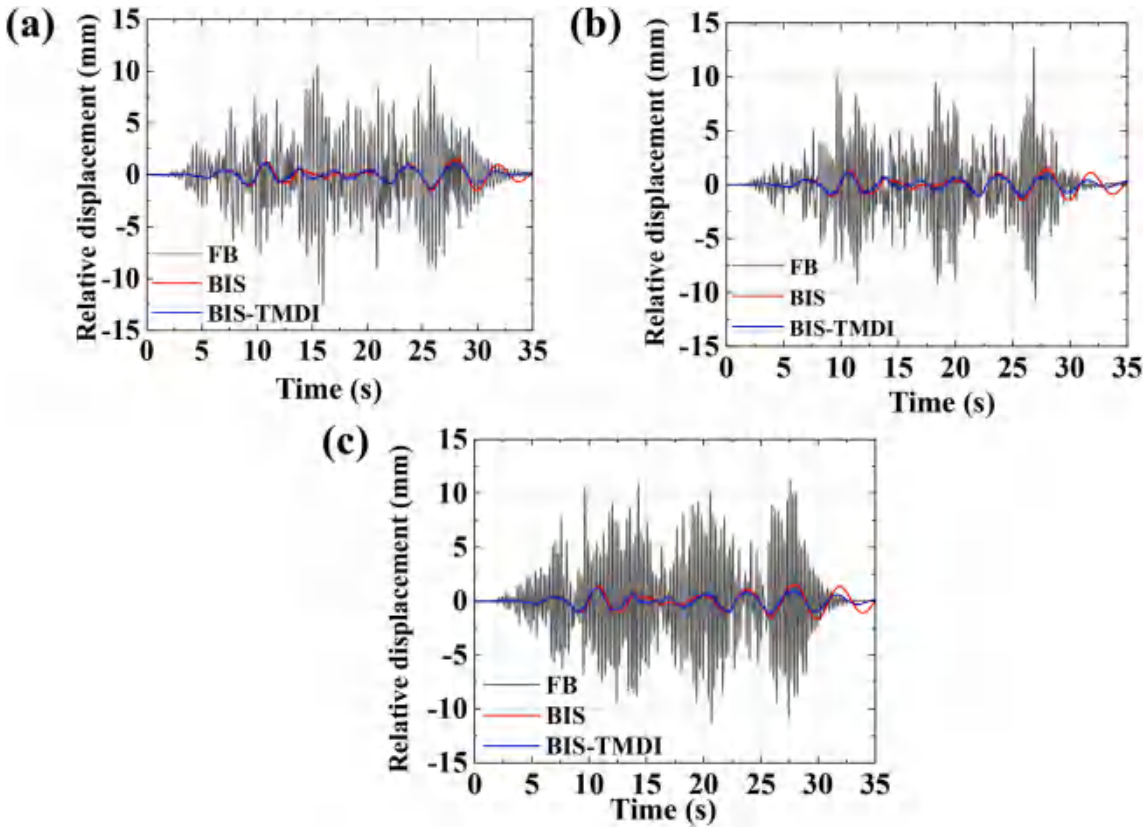

Fig. 18. The relative displacement of the upper structure with different vibration control strategies: (a) $h/H_w = 0.9$; (b) $h/H_w = 0.5$; (c) $h/H_w = 0$.

by the water. In fact, the cooling water works as a damper in the vibration process, which influences the seismic response of NPP structures. In the analysis of the maximum acceleration response of the upper structure, the BIS-TMDI system achieves a maximum optimization effect of 4.86% at a water level ratio of 0.9 compared with that of BIS system as seen in Fig. 21. With the implementation of the BIS strategy, the maximum acceleration of the upper structure exhibits a continuous downward trend as the water level ratio increases. The BIS-TMDI strategy results in an initially increasing trend of maximum acceleration responses, followed by a decreasing trend. It is evident that the BIS-TMDI strategy plays an effective role in the vibration control of the AP1000 NPP structure. Moreover, selecting an appropriate water level ratio would further enhance the vibration control effectiveness of the structure.

5. Conclusion

This paper introduces a BIS-TMDI vibration control strategy to mitigate seismic responses of the AP1000 NPP structure. The influence of water level ratio of the PCCWST on seismic performance of the AP1000 NPP structure is analyzed. A corresponding theoretical model is proposed based on the Housner's model, and it is validated by a series of time history analyses. Three single-objective optimization strategies and one multi-objective optimization strategy are presented to mitigate the seismic responses of NPP structures. Meanwhile, a series of time history analyses are conducted to examine the influence of vibration control

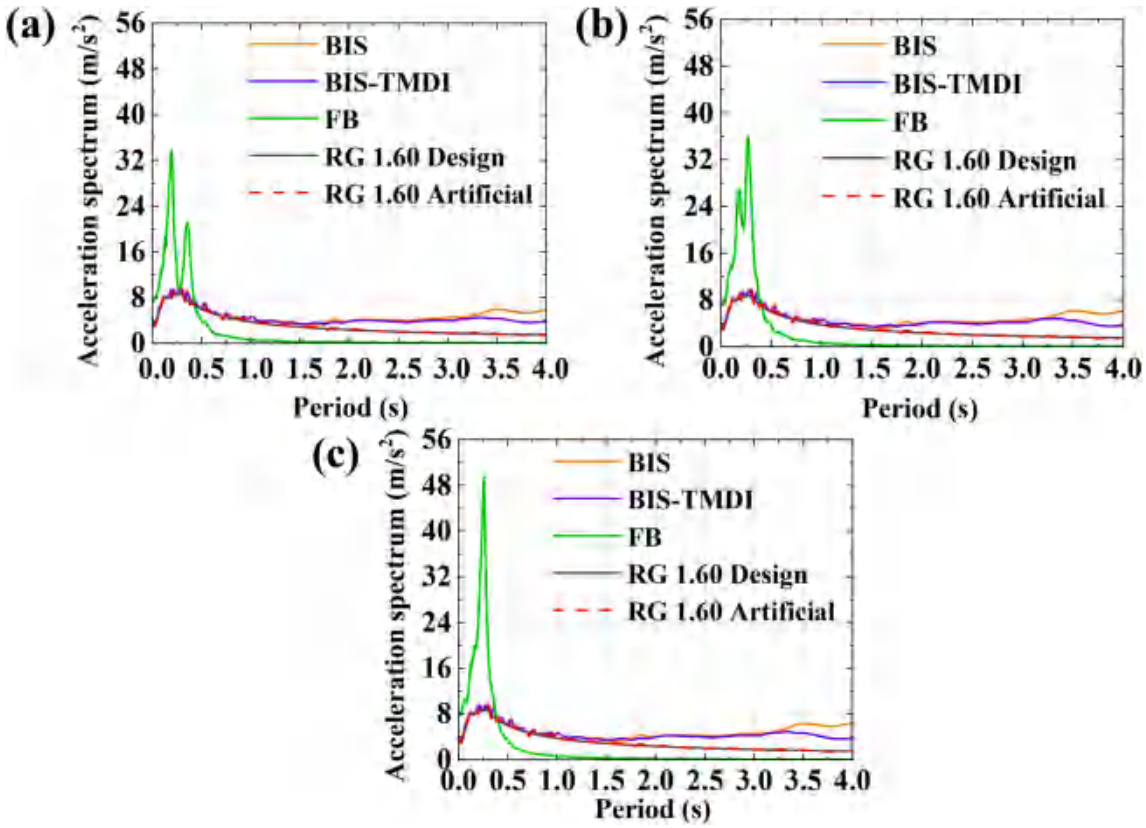

Fig. 19. The acceleration spectrum of the upper structure with different vibration control strategies: (a) $h/H_w = 0.9$; (b) $h/H_w = 0.5$; (c) $h/H_w = 0$.

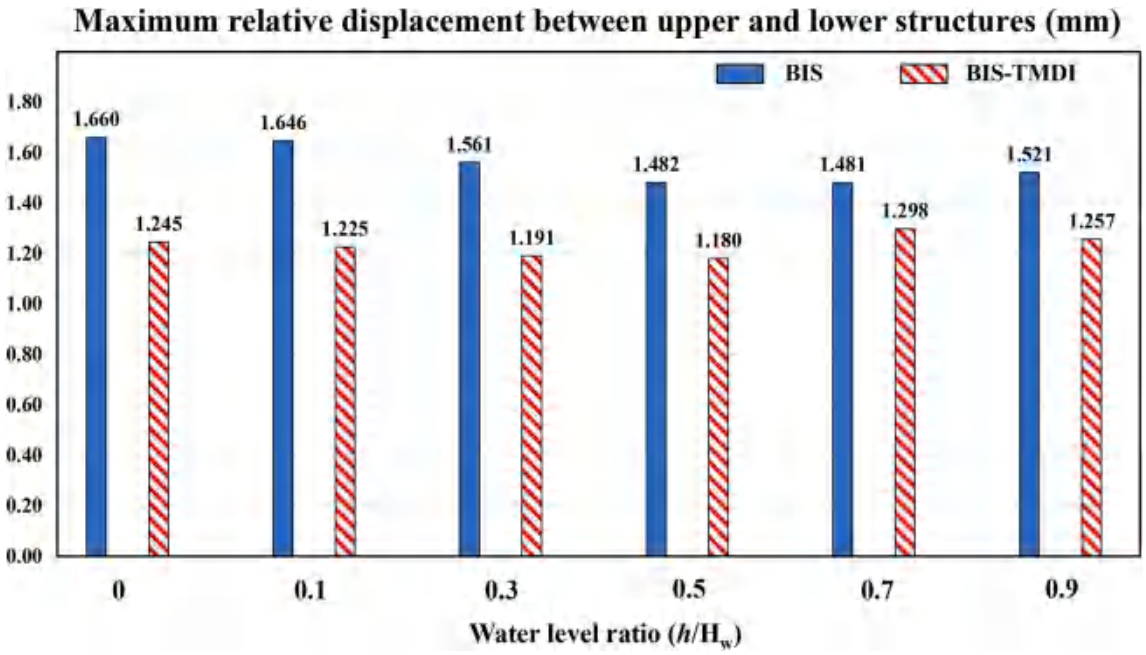

Fig. 20. The maximum relative displacement with varying water level ratios.

strategies on seismic performance of the AP1000 NPP structure with various water level ratios. This study provides theoretical insights into seismic mitigation of AP1000 NPP structure, offering significant engineering value and design guidance. The main conclusions are as follows.

- On the condition that the water level ratio of PCCWST is 0.9 and μ_t is designated (0.01, 0.05, 0.1, and 0.2), the optimal frequency ratio ν_{topt} and optimal damping ratio ζ_{topt} exhibit creep changes with the increasing β_t. This phenomenon occurs while aiming to minimize the relative displacement variance and absolute acceleration variance of the upper structure, as well as the FEI. By selecting an appropriate

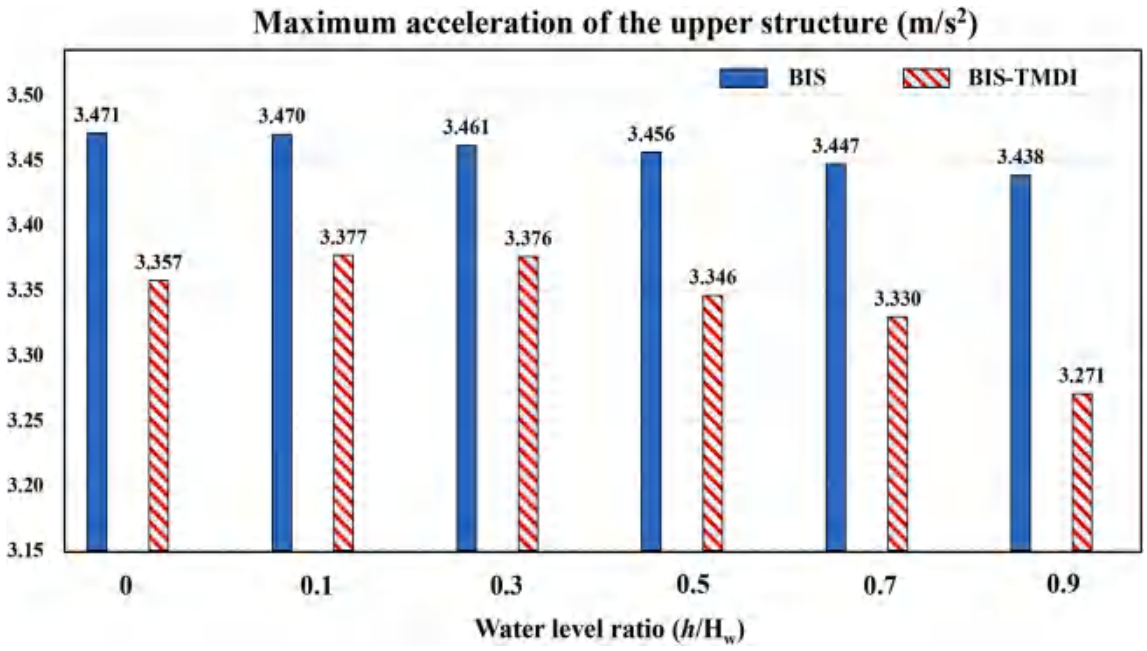

Fig. 21. The maximum acceleration of the upper structure with varying water level ratios.

value of β_t, effective vibration reduction of AP1000 NPP structure is achieved in engineering design. Meanwhile, both the optimal frequency ν_{topt} and optimal damping ratio ζ_{topt} are obtained, which make the practice common.

- Compared with the BIS strategy, the hybrid vibration control BIS-TMDI strategy is beneficial to significantly reduce the seismic response of the AP1000 NPP structure. When the AP1000 NPP structure is subjected to the RG1.60 artificial wave, the maximum displacement difference between the upper structure and lower structure is optimized by 25.45%, and the maximum acceleration of the upper structure is reduced by 4.86%.
- In the proposed BIS-TMDI strategy, the maximum relative displacement response of the upper structure is most unfavorable when the water level ratio is 0.7, while the maximum acceleration of the upper structure is highest at a water level ratio of 0.1. This phenomenon arises due to the varying water level ratios, which change the fundamental frequency of the AP1000 structure. Meanwhile, the water oscillation influences the seismic performance of NPP structures. Hence, selecting an appropriate water level ratio contributes to enhancing the vibration control effectiveness of the AP1000 structure.

Funding

This work was supported by Heilongjiang Provincial Key Research and Development Plan funded by Heilongjiang Province, China (Department of Science and Technology) (Grant No. 2022ZX01A14), and Leading Scientific Research and Young Talent Project funded by China National Nuclear Corporation, China (Grant No. KY90200210017), and Yantai School-Local Integration Development Program funded by Yantai City, China (Grant No. 22MZ03CD012).

Declaration of competing interest

We declare that we do not have any commercial or associative interest that represents a conflict of interest in connection with the work submitted.

References

[1] L. Tuñón-Sanjur, R.S. Orr, S. Tinic, et al., Finite element modeling of the AP1000 nuclear island for seismic analyses at generic soil and rock sites, Nucl. Eng. Des. 237 (12) (2007) 1474–1485.
[2] M. Kawashima, T. Sawano, M. Murakami, et al., Association between the deaths indirectly caused by the Fukushima Daiichi nuclear power plant accident (disaster-related deaths) and pre-disaster long-term care certificate level: a retrospective observational analysis, Int. J. Disaster Risk Reduc. 96 (2023) 103989.
[3] A.S. Whittaker, M. Kumar, M. Kumar, Seismic isolation of nuclear power plants, Nucl. Eng. Technol. 46 (5) (2014) 569–580.
[4] H.-B. Surh, T.-Y. Ryu, J.-S. Park, et al., Seismic response analysis of a piping system subjected to multiple support excitations in a base isolated NPP building, Nucl. Eng. Des. 292 (2015) 283–295.
[5] R. Lo Frano, G. Forasassi, Isolation systems influence in the seismic loading propagation analysis applied to an innovative near term reactor, Nucl. Eng. Des. 240 (10) (2010) 3539–3549.
[6] N. Ostrovskaya, Y. Rutman, Optimum control of energy dissipation in support-pendulum seismic isolation system for large NPP equipment, Procedia Struct. Integr. 6 (2017) 19–26.
[7] J.M. Kelly, S. Dynamics, The role of damping in seismic isolation, Earthq. Eng. Struct. Dynam. 28 (1999) 3–20.
[8] F. Hermann, Device for Damping Vibrations of Bodies [J], 1911.
[9] T. Taniguchi, A. Der Kiureghian, M. Melkumyan, Effect of tuned mass damper on displacement demand of base-isolated structures, Eng. Struct. 30 (12) (2008) 3478–3488.
[10] M. Azeem, A.S. Sajith, P.V. Indira, Response control of base-isolated structures using tuned-mass dampers—a numerical study, in: Proceedings of the Recent Advances in Materials, Mechanics and Structures, Springer Nature Singapore, Singapore, F, 2023 [C].
[11] L. Wang, S. Nagarajaiah, W. Shi, et al., Seismic performance improvement of base-isolated structures using a semi-active tuned mass damper, Eng. Struct. 271 (2022) 114963.
[12] S. Kwag, S. Eem, J. Kwak, et al., Mitigation of seismic responses of actual nuclear piping by a newly developed tuned mass damper device, Nucl. Eng. Technol. 53 (8) (2021) 2728–2745.
[13] I.F. Lazar, S.A. Neild, D.J. Wagg, Using an inerter-based device for structural vibration suppression, Earthq. Eng. Struct. Dynam. 43 (8) (2014) 1129–1147.
[14] M.C. Smith, Synthesis of mechanical networks: the inerter, IEEE Trans. Automat. Control 47 (10) (2002) 1648–1662.
[15] L. Marian, A. Giaralis, Optimal design of a novel tuned mass-damper–inerter (TMDI) passive vibration control configuration for stochastically support-excited structural systems, Probabilist. Eng. Mech. 38 (2014) 156–164.
[16] M. De Angelis, A. Giaralis, F. Petrini, et al., Optimal tuning and assessment of inertial dampers with grounded inerter for vibration control of seismically excited base-isolated systems, Eng. Struct. 196 (2019) 109250.
[17] D. De Domenico, G. Ricciardi, An enhanced base isolation system equipped with optimal tuned mass damper inerter (TMDI), Earthquake engineering and structural dynamics 47 (5) (2018) 1169–1192.
[18] D. Pietrosanti, M. De Angelis, A. Giaralis, Experimental study and numerical modeling of nonlinear dynamic response of SDOF system equipped with tuned

mass damper inerter (TMDI) tested on shaking table under harmonic excitation, Int. J. Mech. Sci. 184 (2020) 105762.
[19] D. Pietrosanti, M. De Angelis, A. Giaralis, Experimental seismic performance assessment and numerical modelling of nonlinear inerter vibration absorber (IVA)-equipped base isolated structures tested on shaking table, Earthq. Eng. Struct. Dynam. (10) (2021) 2732–2753.
[20] J. Bian, X. Zhou, K. Ke, et al., Seismic resilient steel substation with BI-TMDI: a theoretical model for optimal design, Journal of Constructional Steel Research 192 (2022) 107233.
[21] C. Zhao, N. Yu, Y.L. Mo, Seismic fragility analysis of AP1000 SB considering fluid-structure interaction effects, J]. Structures 23 (2020) 103–110.
[22] Q. Xu, J. Chen, C. Zhang, et al., Dynamic analysis of AP1000 shield building considering fluid and structure interaction effects, Nucl. Eng. Technol. 48 (1) (2016) 246–258.
[23] Y. Jiang, Z. Zhao, R. Zhang, et al., Optimal design based on analytical solution for storage tank with inerter isolation system, Soil Dynam. Earthq. Eng. 129 (2020) 105924.
[24] C. Luo, H. Mu, H. Wang, et al., Study on the seismic mitigation effects of inerter isolated storage tanks, Soil Dynam. Earthq. Eng. 173 (2023) 108140.
[25] Z.D. Labaf, D.M. Angelis, M. Basili, Multi-objective optimal design and seismic assessment of an inerter-based hybrid control system for storage tanks, Bull. Earthq. Eng. 21 (3) (2023) 1481–1507.
[26] L. Zhang, M. Guo, Z. Li, et al., Optimal design and seismic performance of base-isolated storage tanks using friction pendulum inerter systems, Structures 43 (2022) 234–248.
[27] C. Zhao, J. Chen, Q. Xu, FSI effects and seismic performance evaluation of water storage tank of AP1000 subjected to earthquake loading, Nucl. Eng. Des. 280 (2014) 372–388.
[28] Z. Zhang, C. Song, Z. Duan, et al., Experimental and numerical studies of AP1000 shield building considering fluid-structure interaction, Science and Technology of Nuclear Installations 2022 (2022) 6458549.
[29] D. Wang, C. Wu, W. Huang, et al., Vibration investigation on fluid-structure interaction of AP1000 shield building subjected to multi earthquake excitations, Ann. Nucl. Energy 126 (2019) 312–329.
[30] F. Naeim Ph D, S.E. J, M. Kelly Ph D, Theoretical Basis of Seismic Isolation [M], Design of Seismic Isolated Structures, 1999, pp. 25–45.
[31] Z. Zhao, Q. Chen, R. Zhang, et al., Optimal design of an inerter isolation system considering the soil condition, J]. Engineering Structures 196 (2019) 109324.
[32] C. Song, X. Li, G. Zhou, et al., Research on FSI effect and simplified method of PCS water tank of nuclear island building under earthquake, Prog. Nucl. Energy 100 (2017) 48–59.
[33] D. Lu, Y. Liu, X. Zeng, Experimental and numerical study of dynamic response of elevated water tank of AP1000 PCCWST considering FSI effect, Ann. Nucl. Energy 81 (2015) 73–83.
[34] M. Kumar, A.S. Whittaker, M.C. Constantinou, Extreme earthquake response of nuclear power plants isolated using sliding bearings, Nucl. Eng. Des. 316 (2017) 9–25.
[35] D. Wang, C. Zhuang, Y. Zhang, Seismic response characteristics of base-isolated AP1000 nuclear shield building subjected to beyond-design basis earthquake shaking, Nucl. Eng. Technol. 50 (1) (2018) 170–181.
[36] Z. Zhao, X. Hu, R. Zhang, et al., Advantages and Design of Inerters for Isolated Storage Tanks Incorporating Soil Conditions, 2023.
[37] J. Song, K. Bi, R. Ma, et al., Vibration control of adjacent structures equipped with inerter-based dampers considering nonlinearities: analytical and experimental studies, Mech. Syst. Signal Process. 206 (2024) 110903.
[38] R. Jangid, Performance of Supplemental inertial devices for base-isolated structures, in: Proceedings of the ASPS Conference Proceedings, F, 2022 [C].
[39] J.-H. Park, H.M. Koh, J.K. Kim, Seismic isolation of pool-type tanks for the storage of nuclear spent fuel assemblies, Nucl. Eng. Des. 199 (1) (2000) 143–154.
[40] A.K. Gupta, T. Hassan, A. Gupta, Correlation coefficients for modal response combination of non-classically damped systems, Nucl. Eng. Des. 165 (1) (1996) 67–80.
[41] D. Pietrosanti, M. De Angelis, M. Basili, Optimal design and performance evaluation of systems with tuned mass damper inerter (TMDI), Earthq. Eng. Struct. Dynam. 46 (8) (2017) 1367–1388.
[42] Y. Chen, C. Xiong, T. Ma, et al., Research on Floor response spectrum of shielded building structure under seismic loading, IOP Conf. Ser. Earth Environ. Sci. 446 (2) (2020) 022001.
[43] A. Seismoartif, New tool for artificial accelerograms generation. http://www.seismosoft.com, 2013.